CHAPTER 3

Similarity and dissimilarity in air–sea momentum and CO_2 transfers: the nondimensional transfer coefficients in light of the windsea Reynolds number

Y. Toba[1,2,3], S. Komori[4], Y. Suzuki[5] & D. Zhao[6]
[1]*Tohoku University (Emeritus), Japan.*
[2]*Earth Observation Research Center, National Space Development Agency of Japan (EORC/NASDA), Japan.*
[3]*Research Institute for Environmental Sciences and Public Health of Iwate Prefecture (I-RIEP), Japan.*
[4]*Department of Mechanical Engineering and Advanced Research Institute of Fluid Science and Engineering, Kyoto University, Japan.*
[5]*Research Department, Japan Weather Association, Japan.*
[6]*Physical Oceanography Laboratory, Ocean University of China, China.*

Abstract

From dimensional considerations it is deduced that in *wind–windsea equilibrium* the fluid dynamical conditions can be described by only two nondimensional parameters. One is the wave age for the representative windsea. This describes the degree of windsea development relative to the local wind. The other is the *windsea Reynolds number* R_B, which is defined by $u_*^2/\nu\sigma_p$, where u_* is the air friction velocity, ν is the air kinematic viscosity, and σ_p is the angular frequency at the windsea spectral peak. R_B was introduced by Toba and Koga in 1986, and formerly it was denoted as the *breaking-wave parameter*. It is the fundamental controlling parameter for the *windsea boundary layer*, and consequently for the behavior of air–sea transfers. R_B is shown to be much superior to the 10-m wind speed, U_{10} or u_*, in studying the behavior of transfer coefficients.

The air–sea CO_2 transfer has traditionally been expressed in terms of a transfer velocity k_L as a function of U_{10}. We propose the use of a nondimensional transfer

WIT Transactions on State of the Art in Science and Engineering, Vol 23, © 2006 WIT Press
www.witpress.com, ISSN 1755-8336 (on-line)
doi:10.2495/978-1-85312-929-2/03

velocity k_L/U_{10}, motivated by the drag coefficient C_D for the momentum transfer. Existing data show that there is fundamental similarity in the behavior of these nondimensional coefficients, with some dissimilarity in a range of R_B. Detailed findings are as follows.

1. Though C_D generally increases with R_B, laboratory data show two troughs, or critical points at $R_B = 2 \times 10^2$ and 10^3, with a flat bulge region in between. The first trough corresponds to the transition from the region where tangential stress prevails to the occurrence of airflow separation and reattachment to create the form drag. $R_B = 10^3$ is a conspicuous critical point beyond which windsea breaking occurs on the fully rough water surface, namely it is the transition to the full turbulence regime of the windsea boundary layer.
2. Between $R_B = 2 \times 10^2$ and 10^3, k_L/U_{10} decreases. The reason is that in gas transfer processes, the mechanism corresponding to the pressure–force for the momentum transfer is not available.
3. Field data, under the usual swell conditions, show smaller values or a remarkable shift of the second critical point to larger values in R_B, for both the nondimensional transfer coefficients. This corresponds to the fact that windsea energy becomes small in the presence of swell in some conditions, causing the sea surface to be dynamically smoother.
4. Distributions of data points from windsea tank experiments and from field experiments coincide with each other on the C_D vs. k_L/U_{10} and the C_D vs. k_L diagrams.

We propose further studies of the behavior of the nondimensional air–sea CO_2 transfer coefficient, as well as C_D, as a function of R_B, under various swell conditions, and for unsteady winds, in order to match the contemporary evolution of oceanic data sets with powerful new numerical simulations and ocean-wave models that are presently being generated.

1 Introduction

Coupled atmosphere–ocean models have made remarkable progress in recent years. In associated observational programs for global oceans, a new system of Argo floats are being deployed, which will collect 3000 CTD data points a day over the worlds' oceans. Moreover, enhanced satellite observations and a four-dimensional assimilation system, which the Global Data Assimilation Experiment (GODAE) will develop, are opening a new age of oceanography, a data revolution. In this new age, estimates of air–sea fluxes, including momentum and gas transfers, appear out of date, using only the 10-m wind speed and the air–sea partial pressure difference for gas transfers, respectively, neglecting the effect of sea state. With regard to the latter, Soloviev and Schlüssel [1] and others have proposed the necessity of sea-state dependence if gas transfer estimates are to be improved.

This chapter considers the challenge of determining a better parametrization to estimate the global CO_2 transfer between the atmosphere and the oceans, in light of

laminar–turbulent regimes at the air–sea interface, which are greatly related to local wind and *wind waves*. Hereafter, we will use the term *windsea* for *wind waves*, after the terminology of Csanady [2], to express special fluid dynamical phenomena of wind waves, such as nonlinear coupling of water waves with local wind drift and turbulence, caused by the wind at the air–sea interface (cf. Toba [3, 4]). Regarding processes related to momentum and the gas transfers, both the skin friction and the form drag are important for the momentum transfer, whereas for the gas transfers the mechanism corresponding to the form drag is missing and contamination by small surface-active impurities is an important factor. However, in both cases the transfers are driven by turbulence rather than mere interface transfers. Wind-wave breaking, including incipient breaking, is closely related to the surface renewal as well as to the state of turbulence.

Toba and Koga [5] proposed the breaking-wave parameter R_B to systematically describe various air–sea boundary processes. R_B is defined by $u_*^2/\nu\sigma_p$, where u_* is the air friction velocity, ν is the kinematic viscosity of air, and σ_p is the windsea spectral peak frequency. In this chapter, we rename R_B the *windsea Reynolds number*, since it is, from dimensional considerations, the only fundamental Reynolds number to describe fluid dynamical similarity conditions for *windsea boundary layer* phenomena, under the conditions of *wind–windsea equilibrium*. From observational data analyses, R_B has already proven very effective in expressing the windsea breaking rate (Toba and Koga [5]), the whitecap coverage (e.g., Zhao and Toba [6]), and sea-spray droplet production (Iida *et al*. [7]). We will consider the behavior of the transfer coefficients for momentum and CO_2.

We briefly review the present status of the transfer coefficients: momentum transfer in Section 2.1 and CO_2 transfer velocity k_L in Section 2.2. Then, in Section 3.1 we present a review of the wind–windsea equilibrium dynamics resulting in the similarity laws for windsea, the 3/2-power law, and in Section 3.2, using nondimensional analyses, we show that a single representative parameter can describe the windsea state itself, or the wave age. We also show the importance of R_B in describing the associated fluid dynamical similarity for the air–sea boundary layer including pure windsea phenomena. We review the past data on availability of R_B for wave-breaking related phenomena in Section 3.3. In Section 4 we present a new description of the behavior of the drag coefficient C_D in light of R_B, and we provide motivation for its interpretation as the *windsea Reynolds number*. We will point out that the traditional transfer coefficients, as functions only of the wind speed and of the air–sea partial pressure difference for gases, are unstable quantities by themselves, because of dominating nonequilibrium conditions: dynamical contamination such as swells and the unsteady winds. In Section 5 we present new findings with respect to the similarity between the behavior of C_D and k_L from the viewpoint of R_B, using observational data. We give physical interpretations, as far as possible, to propose a new *nondimensional CO_2 transfer velocity*.

Finally, we propose further studies of the nondimensional transfer coefficients, to provide better estimates of global air–sea transfers appropriate for this age of the ocean data revolution. We also briefly discuss the outstanding questions that remain to be investigated.

2 Present status of air–sea transfer coefficients

2.1 Momentum transfer (drag) coefficient

Historically, the sea-surface wind stress, τ, was expressed by

$$\tau = \rho C_{\mathrm{D}} U_{10}^2 \ (=\rho u_*^2), \tag{1}$$

where ρ is the density of the air, C_{D} is a dimensionless drag coefficient, and U_{10} is the 10-m wind speed. This equation actually defines C_{D} and the air friction velocity u_*.

The original meaning of eqn (1) is

$$\tau = C_{\mathrm{D}} \Delta M U_{10}, \quad \Delta M = \rho U_{10}, \tag{2}$$

where ΔM is the difference of air momentum between the 10-m level and the sea surface, and it is assumed that τ should be proportional to both ΔM and U_{10}. For a solid surface, C_{D} is actually a constant of the order of 10^3, differing according to the nature of the surfaces. Windsea exists at the air–sea boundary, and observations have shown that C_{D} is not a constant but highly variable, even under neutral stratification conditions. It has traditionally been assumed that this scatter may be expressed as a function of U_{10}. However, C_{D} should actually be a measure that extracts (or amplifies) delicate variations due to the unsteady wind and the state of windsea, though observational errors are also being amplified.

A series of recent observations have shown a compact distribution. An example is a formula presented by Yelland *et al.* [8], expressed as

$$10^3 C_{\mathrm{DN}} = (0.50 \pm 0.02) + (0.071 \pm 0.002) U_{10\mathrm{N}} \quad (6 < U_{10\mathrm{N}} < 26\,\mathrm{m/s}), \tag{3}$$

where the subscript N indicates neutral stratification. This data was obtained by the inertial dissipation method in deep water, with a correlation coefficient of 0.80 for 1111 data points. However, there was considerable scatter among individual measured values (e.g., Yelland and Taylor [9], their fig. 7.5). This scatter was considered to be caused by the effect of windsea, in seas ranging from young to old, and swells.

There have been many attempts to determine the cause of the data scatter, but they have not been fully successful. Figure 1 shows one of these recent efforts. It is a synthesis of observational data from laboratory experiments as well as open ocean data, with an overall parametrization proposed by the SCOR Working Group 101 (Jones and Toba [10]). The data are expressed in terms of the nondimensional roughness parameter (gz_0/u_*^2) as a function of the inverse wave age $\beta^{-1} = (u_*/C_{\mathrm{p}})$, where g is the acceleration due to gravity, z_0 is the aerodynamic roughness parameter (associated with the neutral stratification C_{D}), and C_{p} is the phase speed of the wind-wave peak frequency. The latter represents the state of windsea conditions. The SCOR formula was expressed as

$$\begin{aligned} gz_0/u_*^2 &= 0.03\beta \exp(-0.14\beta), \quad \sim 0.35 < \beta < 35 \\ &= 0.008, \quad \beta \geq 35 \text{ (light winds over swell).} \end{aligned} \tag{4}$$

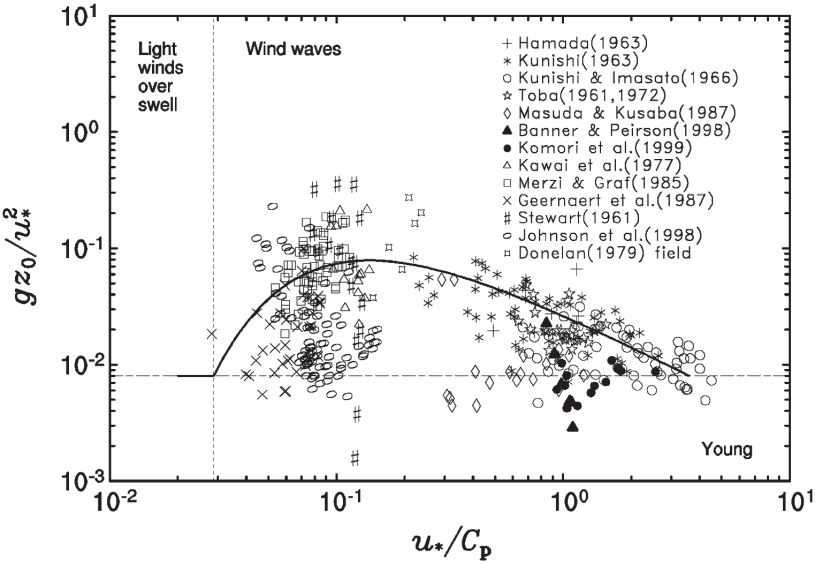

Figure 1: A synthesis of sea-surface drag data observed at laboratories and seas. The data are expressed in terms of the nondimensional roughness parameter (gz_0/u_*^2) as a function of the inverse wave age $\beta^{-1} = (u_*/C_p)$. An overall formula [eqn (4)] proposed by the SCOR Working Group 101 is shown as a thick curve. The figure is from Jones and Toba [10] with some additional recent data. The right hand cluster of data points are from laboratory experiments and the left hand cluster are from field observations.

The Jones and Toba [10] SCOR report presented comprehensive reviews on various effects that can cause the scattering in measurements of C_D. These included the presence of windsea and swell, unsteady winds, atmospheric boundary layer rolls, large time and space averages of data, surface tension biases in observations, spatial inhomogeneity, basin boundaries, and the effect of stability, constituting another important atmospheric boundary layer factor. Recent data taken at a tower station by Suzuki *et al.* [11] showed that crosswind swells also significantly reduced C_D.

2.2 CO_2 transfer velocity

The CO_2 flux F through the water surface has usually been expressed by:

$$F = k_L S \Delta pCO_2, \tag{5}$$

where k_L is the gas exchange coefficient, S is the solubility of the gas, and ΔpCO_2 is the difference between the partial pressures of the gas in air and in water. The value of k_L is to be determined empirically. It is important that k_L has the dimensions of speed (m s^{-1}), which is different from the case of C_D.

Although the CO_2 transfer velocity k_L across the air–sea interface has been measured by a number of investigators in oceans and lakes (McGillis *et al.* [12]; Fairall *et al.* [13]; Haubecker and Jahne [14]; Wanninkhof *et al.* [15]; Watson *et al.* [16]; Cember [17]; Broecker *et al.* [18]), the field data for k_L plotted against U_{10} are very scattered among individual studies. The scatter may have been caused by factors such as windsea, swell, density stratification, surfactants, bubbles, and so on (e.g., Komori and Shimada [19]; Komori and Misumi [20]).

However, one of the biggest problems in previous studies was that the scattered k_L data were usually correlated by monotonous increasing curves with U_{10} (e.g., Liss and Merlivat [21]; Wanninkhof [22]) and the validity of the correlation with U_{10} has not been physically discussed.

The CO_2 transfer across the air–sea interface is controlled by a laminar–turbulent regime shift of the windsea boundary. Turbulent motions on the liquid side beneath the interface are especially important. Komori *et al.* [23] first verified that surface-renewal eddies on the water side control heat transfer across the air–water interface. The significant role of surface-renewal eddies on the CO_2 transfer has been confirmed in both an open channel flow with an unsheared air–water interface (Komori *et al.* [24]) and a wind-driven turbulence with a sheared interface (Komori *et al.* [25]). These studies have found that k_L follows the surface-renewal concept in the low and middle wind speed region without wave breaking. That is, k_L is proportional to the square root of the frequency of appearance of surface-renewal eddies $f_s^{1/2}$. In addition, Komori *et al.* [26] showed that k_L remarkably increases in the wave-breaking region, since the effect of very tiny surfactants disappears owing to wave breaking. These results suggest that k_L should be correlated not solely with the wind speed but with a parameter that should be constituted by the surface-renewal frequency f_s, and also the wave-breaking ratio. However, it is almost impossible to estimate the surface-renewal frequency directly from available remotely sensed observational data, and therefore we have to find a new parameter that reflects both the turbulence structure and the wave-breaking occurrence.

A recent paper by Zhao *et al.* [27] is one effort in this direction. We will present a further comprehensive effort in Section 5.

3 Wind–windsea equilibrium and nondimensional windsea boundary layer variables

3.1 Wind–windsea equilibrium: similarity laws of windsea

Nonlinear interactions between the wind and the windsea are very strong. They include turbulence, shear flows, the form drag and breaking of the air–water interface, and the related microphysical processes at the air–water interface, together with the breaking of waves themselves. As a result of these strong interactions, there are statistical similarity laws particular to the windsea field. In this section, these similarity laws are briefly reviewed. The similarity laws give a basis for the pure windsea field being expressed by using a single nondimensional parameter,

and also for the importance of the windsea Reynolds number. A detailed review of these similarity laws is given by Toba [3, 4, 28].

3.1.1 The 3/2-power law

For growing windsea under steady wind conditions, i.e., for windsea in local equilibrium with the wind, there exists the 3/2-power law which is expressed as:

$$H^* = BT^{*3/2}, \quad B = 0.062, \tag{6}$$

where $H^* = gH_s/u_*^2$ and $T^* = gT_s/u_*$, H_s is the significant wave height, T_s is the significant wave period, and B is an empirical constant. Alternatively, eqn (6) may be expressed in a dimensional form:

$$H_s = B(gu_*)^{1/2}T_s^{3/2}. \tag{7}$$

Equation (6) compares well with data as seen from fig. 2–6 of Toba [28], or fig. 23 of Toba [4]. Ebuchi *et al.* [29] showed that the 3/2-power law with the above value of B holds even for cases with some swells, though not under dominant swells (see also Johnson *et al.* [30]).

This power law was originally derived by Toba [31, 32] by eliminating nondimensional fetch from empirical formulas for the growth of wind waves, e.g., as given by Wilson [33], Mitsuyasu *et al.* [34], and the JONSWAP formula by Hasselmann *et al.* [35]. However, the 3/2-power law is not a consequence of fetch laws for each of H_s and T_s, but of the local equilibrium between the wind and windsea, where H_s and T_s are intrinsically related to u_*.

As a matter of fact, it was already shown that eqn (6) is just equivalent to the condition of proportionality

$$u_* \propto (\overline{u_a'^2})^{1/2} \propto (\overline{u_w'^2})^{1/2} \propto u_{*w} \propto u_0, \tag{8}$$

where $(\overline{u_a'^2})^{1/2}$ is the intensity of air turbulence, $(\overline{u_w'^2})^{1/2}$ is the intensity of water turbulence, u_{*w} is the water friction velocity, and u_0 is the Stokes drift velocity (see Toba [3, 28, 32]).

Fetch is usually difficult to define in the oceans, since the winds are always varying. Nevertheless the 3/2-power law holds, especially for strong wind cases, or for cases free of dominant swells (Ebuchi *et al.* [29]). Also, Wilson's fetch graph formulae [33] show that the 3/2-power law holds for conditions approaching long-fetch saturation, where the empirical fetch laws for the nondimensional H_s and T_s have complicated forms.

In the sea, the value of B was estimated as $0.062 \pm 20\%$ by Toba *et al.* [36] as derived from measured data. The scatter is largely due to unsteady winds, namely conditions where windsea is not in local equilibrium with the wind, and the windsea is over- or undersaturated (Toba *et al.* [37, 38]; Waseda *et al.* [39]). The influence of unsteady winds on the wind stress was reviewed in chapter 9 of Jones and Toba [10]. Komatsu and Masuda [40] numerically estimated Toba's constant B to have a "standard" value of 0.06, using the RIAM method to numerically evaluate

nonlinear energy transfers among wind waves, as well as by using the WAM method (The WAMDI Group [41]). Suzuki [42] reported some similar results by using his JWA3G wave model.

Alternatively, the 3/2-power law can be regarded as the situation where the steepness of significant waves is statistically limited, as a function of the wave age of significant waves $\beta = C_s/u_*$, as an equilibrium state of windsea under the action of the local wind. This relation is expressed by

$$\frac{H_s k_s}{2\pi} = (2\pi)^{1/2} B \left(\frac{C_s}{u_*}\right)^{-1/2} \left\{1 + u_s^* \left(\frac{C_s}{u_*}\right)^{-1}\right\}^{-2/3}, \quad u_s^* \equiv \frac{u_s}{u_*} = 0.206, \quad (9)$$

where k_s is the significant wave number, C_s the phase speed of significant waves, and u_* is the friction velocity of air (Bailey *et al.* [43]). The wave age in the second term is the consequence of an averaged local wind drift u_s (Tokuda and Toba [44]).

3.1.2 One-dimensional windsea frequency spectral form

In observed windsea, there is an equilibrium range in the main part of the high frequency side of the energy spectrum. The accepted one-dimensional windsea frequency spectrum for this range, proposed by Toba [45] from observational data with some dimensional considerations, is given by

$$\phi(\sigma) = \alpha_s g u_* \sigma^{-4}, \quad \sigma > \sigma_p, \quad (10)$$

where α_s is a constant, σ is the angular frequency, and σ_p is the peak angular frequency of windsea. This spectral form has been shown to be consistent with many observational data sets since Kawai *et al.* [46] and Phillips [47] reproposed this form theoretically. Examples of observed data are seen in fig. 2–8 of Toba [28].

Zakharov and Filonenko [48] predicted theoretically that the one-dimensional spectral form should be proportional to σ^{-4} for surface gravity wave interactions. However, there seems to be no study which derives the u_*-proportionality purely from theory. The u_*-proportionality is the most important observational fact for windsea, and the 3/2-power law corresponds to the integral form of this spectral form.

The value of the coefficient α_s seems to be in the range $6 - 12 \times 10^{-2}$ (e.g., Phillips [47]). Joseph *et al.* [49] suggest that α_s should be 0.096 for consistency with the 3/2-power law with $B = 0.062$, for self-similar spectra. However, α_s shows variability in response to the wind fluctuations, just as in the case of B values, corresponding to the over- and undersaturation of the wave energy (Toba *et al.* [38]).

3.1.3 Physical implications

The similarity laws are conceptually expressed, for the 3/2-power law, as

$$f_1(H_s, T_s, u_*) = 0, \quad (11)$$

and for the energy spectrum as

$$f_2(\sigma_p, \phi_p, u_*) = 0, \quad (12)$$

where ϕ_p is the spectral density at σ_p and, as a matter of fact, eqn (11) represents the integral form of eqn (12). In any case, specification of two variables, e.g., u_* as the external forcing field and another variable, determines the state of windsea, assuming it is free of dominant swell. As for the physical background of the similarity laws, they are results of a series of wind-forced, strongly nonlinear processes. It is important that the external condition is u_*, and there is u_*-proportionality in the windsea. These laws are the consequence of self-adjustment processes in windsea forced by u_*.

It is noteworthy that Tulin [50] suggested that the 2/3-power law can be explained by a simultaneous consideration of wave energy and wave momentum change rates resulting from wave breaking, keeping the water wave relation:

$$M = E/C, \tag{13}$$

where M is the wave momentum, E is the wave energy, and C is the phase speed. This leads to the necessary downshifting of wave frequency, to satisfy the 2/3-power law, keeping a balance between the wind input and dissipation by wave breaking. Further review of the processes of the local equilibrium is given by Toba [4], Csanady [2], Waseda *et al.* [39], and Toba [28].

The existence of the wind–windsea equilibrium, or the similarity laws, as described in this section provides a basis for our analyses, using the windsea Reynolds number (breaking-wave parameter).

3.2 Fundamental dimensional considerations

The usefulness of nondimensionalizing variables for quantitative analyses of complicated experimental data was comprehensively described in Section 2–1 of Toba [28], together with its practical procedures and applications. By nondimensionalization the number of variables can be reduced by the number of fundamental dimensions originally involved (the Pi theorem), and we can abstract essential characteristics related to the respective phenomenon. The method of nondimensionalization is especially useful for processes where turbulence dominates. In other words, even when experimental data in dimensional quantities are so complex that it is almost impossible to find any law from them, it becomes easy to extract essential relationships or laws by reducing variables in dimensionless forms. However, formal application of the Pi theorem for solely diminishing variables does not tell us how to combine the variables to make nondimensional products, or how to select mutually independent nondimensional variables. In order to construct meaningful nondimensional variables, we must invoke physical insight.

In the case of windsea, the *independent variables* are time and space, or duration and fetch if the wind field is homogeneous. The *dependent variables* are wave property variables such as H_s, T_s, or σ_p, ϕ_p, and u_* as the only *external condition* (or *conditioning variable*), at least under neutral stratification and in the absence of dominant swells. The existence of the similarity laws described in Section 3.1 implies that it is sufficient to select *only one* of these wave-property variables, together with u_*, in order to completely describe the dynamical system.

In terms of *physical constants*, we have the acceleration due to gravity g and the kinematic viscosity of air ν. The viscosity is substantial since the air–sea boundary processes are basically those of a viscous turbulent fluid, and g appears explicitly in eqn (10). Since the kinematic viscosity of water ν_w has a specific ratio with ν, we need consider only ν. We do not need to consider the surface tension, since it is only related to very high frequency waves, and that part of the windsea spectra is actually controlled by u_*, e.g., proportional to $u_*^{2.5}$ (Mitsuyasu and Honda [51]), forming the tail portion of the continuous windsea spectrum.

There are five quantities with two fundamental dimensions of time and length, and we have one relationship [eqn (11) or eqn (6)]. Thus, it is sufficient to construct two fundamental nondimensional variables:

$$H^* = gH_s/u_*^2 \quad \text{or} \quad T^* = gT_s/u_* \quad \text{using eqn (6),} \tag{14}$$

$$R_B = u_*^2/\nu\sigma_p \quad \text{or} \quad u_*^2 T_s/\nu \quad \text{or} \quad u_* H_s/\nu \qquad \text{using eqns (6) and (12).} \tag{15}$$

Here, H^* is interpreted physically as a *measure of the windsea development for a given wind* u_*, since it contains g and H_s (or T_s) in the numerator and u_* in the denominator. The variable R_B is interpreted as a *measure of the fluid dynamical conditions at the air–water boundary*, since u_* and T_s (or inverse σ_p), or H_s, enters both in the numerator. We call this the *windsea Reynolds number*.

As a matter of fact, R_B may be interpreted as a Reynolds number, since it contains u_* as a representative scale of speed, and $L_s = u_* T_s (= 2\pi u_*/\sigma_p)$ as a representative length scale of the phenomenon under consideration. L_s is interpreted as the length representing the distance over which a water particle at the surface is driven by the speed u_* (representing the wind stress) during the representative wave period T_s. For the same value of a Reynolds number Re ($=UL/\nu$ with U and L as the representative scales of speed and length), the equation of motion will have the same solution, even if L, U, and/or ν have different values. This is known as the *Reynolds' similarity law*, which provides the basis for model experiments.

As will be described in Section 3.3, R_B was proposed by Toba and Koga [5] to properly express various air–sea boundary processes including the wind stress, wave breaking, bubble entrainment, and generation of sea-spray droplets, and later Toba *et al.* [52], Zhao and Toba [6], and Toba [28] denoted this variable as the *breaking-wave parameter*. R_B is expected to be closely related to C_D and k_L, as will be discussed later in Section 4. Moreover, it should be noted that T^*, which is related with H^* by the 3/2-power law (6), may be regarded as the *wave age of* the *significant waves*, $\beta = C_s/u_*$, as was earlier pointed out by Toba [31].

3.3 Windsea Reynolds number: fundamental parameter of the windsea boundary layer

To quantify wave breaking, photographs of the sea surface were used to determine the percentage area of whitecap coverage. Most researchers treated it only as a function of the wind: U_{10} or u_* (e.g., Monahan and MacNiocaill [53]; Wu [54]).

In view of the situation that windsea is in local equilibrium with the wind, or has the similarity laws discussed in the previous sections, windsea parameters in addition to wind should be used to describe phenomena related to the air–sea interface. We should invoke the nondimensional analyses as discussed in Section 3.2. Actually, this was done with R_B proposed by Toba and Koga [5]. Figure 2(a) shows the percentage α of breaking crests, among individual waves, passing a fixed point on the water surface, plotted against U_{10}. It is notable that data from short-fetch, wind-wave tank experiments systematically differ from those obtained at a tower station at sea. This shows that α greatly depends on the fetch, which indicates dependence on the degree of windsea development. However, if we plot α against R_B, all the data collapse along a line with an angle of 45°, as shown in Fig. 2(b). We note that α was originally a nondimensional quantity.

Toba and Koga [5] also successfully applied R_B to describe the whitecap coverage, and the sea-spray droplet concentration observed near the sea surface.

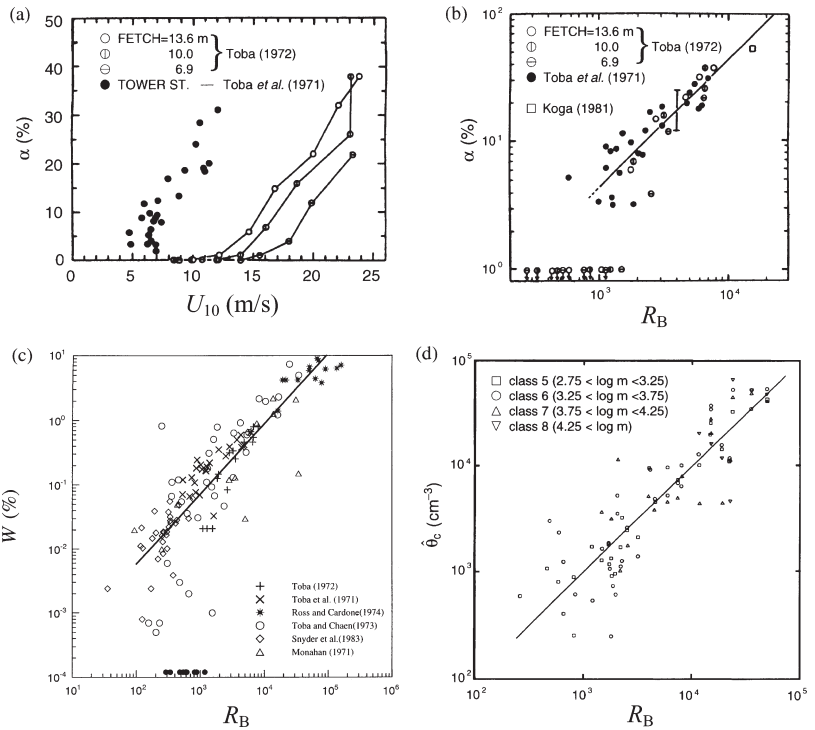

Figure 2: (a) Percentage α of breaking crests among individual waves of windsea passing a fixed point on the water surface, plotted against U_{10}, and (b) plotted against R_B (from Toba and Koga [5]). (c) Whitecap coverage percentage, W, plotted against R_B (from Zhao and Toba [6]). (d) Seawater droplet concentration observed near the sea surface, plotted against R_B (from Iida et al. [7]).

Figure 2(c), from Zhao and Toba [6] with additional data sets, shows that all the data collapses along the 45°-line, and the correlation coefficient is actually 0.88. Wave breaking starts to occur at around $R_B = 10^3$, as suggested by Toba and Koga [5]. Zhao and Toba [6] showed that R_B is the most effective variable, since other variables had correlation coefficients much smaller than R_B, e.g., 0.43 using wave age, and in the cases for H_s, T_s, and u_*, correlation coefficients were not larger than 0.80.

Zhao and Toba [6] also reported that another Reynolds number, $R_H = u_* H_s/\nu$, had a correlation coefficient 0.84. Although this is smaller than 0.88, the variation in the whitecap coverage is similar to R_B, since it is also a Reynolds number representing the same physical processes. In fact, Toba and Kawamura [55] reported that the depth of the associated windsea boundary layer [*downward bursting boundary layer* (*DBBL*)] is 5 times H_s. The concept of this Reynolds number was first used by Toba and Kunishi [56], and later by Banner and Peirson [57]. In using R_B, determination of σ_p may be achieved by taking the peak frequency of the windsea part of the spectra using the methodology proposed by Hanson and Phillips [58]. However, for R_H computations, H_s may be affected by the ever-present existence of swells. Thus R_B is better than R_H as far as wave spectral data are available.

The sea-spray droplet concentration observed near the sea surface also shows a similar distribution, along the 45°-line, as shown in Fig. 2(d) (from Iida *et al.* [7]). Thus the windsea Reynolds number R_B can be considered a crucial parameter for describing macroscopic windsea boundary layer phenomena: windsea breaking, air entrainment, whitecap coverage, and sea-spray droplet (sea-salt particles) production.

Toba and Koga [5] also pointed out the importance of R_B in specifying the sea-surface wind stress. However, we will revisit this matter with a new series of data, in Section 4.

4 Drag coefficient in light of the windsea Reynolds number

As discussed in Section 3, R_B is expected to be a crucial parameter in describing the behavior of nondimensional air–sea transfer coefficients. In this section, we examine it for C_D, and then apply the concept to the CO_2 exchange questions in Section 5.

4.1 Laboratory data: laminar–turbulent boundary layer transition

Figure 3 shows C_D plotted against R_B, as measured by wind-wave tank experiments in fetch-limited (stationary) conditions. The same data set is plotted against U_{10} and against u_* in Fig. 4a and b. These data correspond to conditions where *windsea* is *in local equilibrium with the wind*. These data are the cluster of data points with larger values of u_*/C_p in Fig. 1. The scatter of the data is apparently much smaller in Fig. 3, when expressed as a function of R_B, than when expressed against U_{10} or u_* in Fig. 4a and b. Note that, in the case of Fig. 4b, u_* already includes C_D, after eqn (1). That Fig. 3 shows remarkably better correlation than in Fig. 1 indicates that the wave age is not a proper parameter to discriminate detailed momentum transfer phenomena.

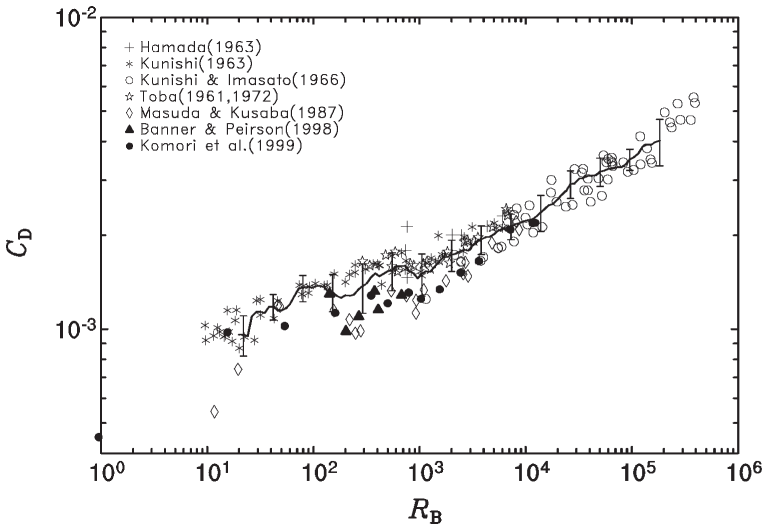

Figure 3: The drag coefficient C_D measured by wind-wave tank experiments in fetch-limited (stationary) conditions plotted against the *windsea Reynolds number* R_B.

An important finding from Fig. 3 is that we can see two critical points in the distribution of C_D, at $R_B = 2 \times 10^2$ and at $R_B = 10^3$. At these points, the data indicate two downward points, which bracket a bulge region. Beyond $R_B = 10^3$, the C_D values become very large. Figure 4a and b does not show any such critical points in a clear-cut way as shown in Fig. 3. The former critical point, $R_B = 2 \times 10^2$, may be regarded as the transition from a smooth surface to the occurrence of airflow separation, and the creation of the form drag. The latter conspicuous critical point, $R_B = 10^3$, corresponds to the transition to the fully turbulent regime of the windsea boundary layer with the occurrence of windsea breaking, as stated in Section 3.3.

As a matter of fact, by using flow visualization techniques Kawai [59, 60] and Kawamura and Toba [61] gave detailed descriptions of the airflow structure over windsea surfaces in a wind-wave tank. Kawamura and Toba [61] demonstrated the existence of a high shear layer at the outer edge of separation bubbles behind laboratory wind-wave crests (their figs 22 and 23). Ebuchi *et al.* [62] described changes of the windsea surfaces from smooth to rough by using an optical method (their fig. 4). Readers can also refer to photographs showing the change of the windsea surfaces in Toba [63], table in Toba [31], and Koga [64]. The conditions of the windsea surfaces, together with the nature of airflow over water, change with the development of windsea as well as with increasing wind speed. Thus, the overall situation should be specified by the *windsea Reynolds number*, R_B.

Regime shifts of these conditions as a function of R_B are shown schematically in Fig. 5. The top panel shows the conditions where the windsea surface is smooth and R_B is small, corresponding to the leftmost part of Fig. 3 (R_B smaller than 10^1). The second panel in Fig. 5 illustrates the conditions for the presence of a separation

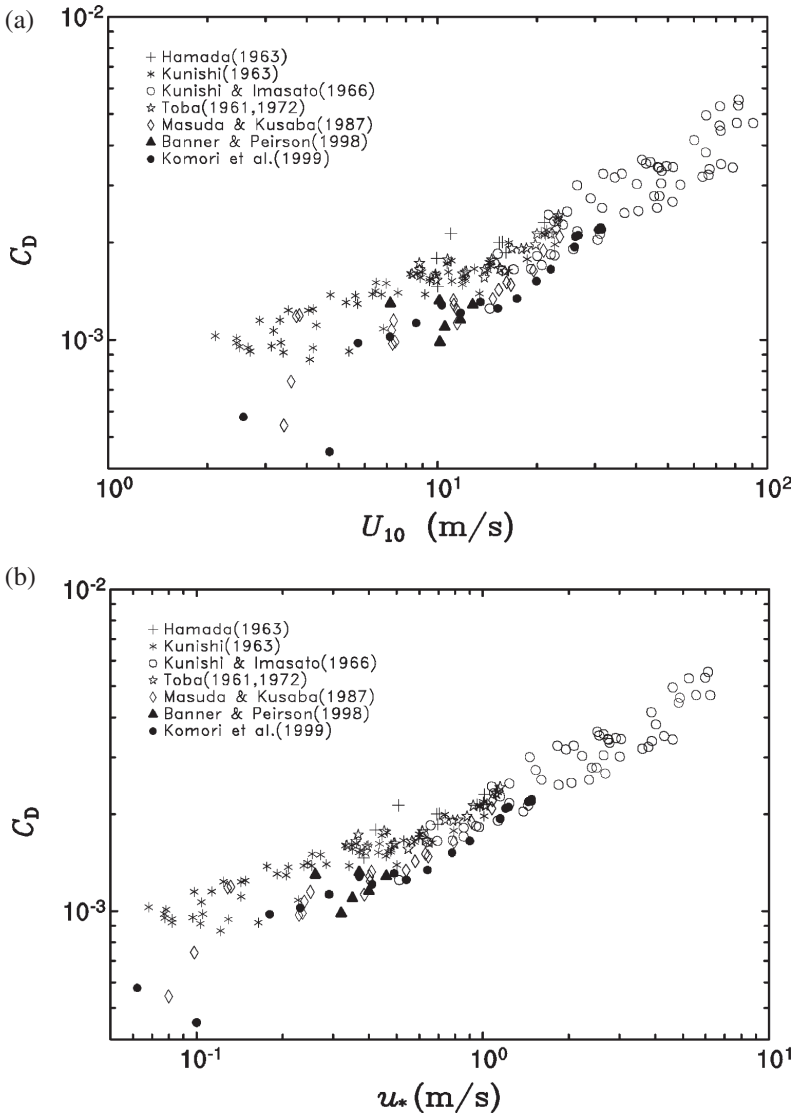

Figure 4: The same data as in Fig. 3 for the drag coefficient C_D measured by wind-wave tank experiments in fetch-limited (stationary) conditions, but plotted against (a) U_{10} and (b) u_*.

point just at the lee side of the crest (about 3×10^2 in R_B), corresponding to figs 22 and 23 of Kawamura and Toba [61]. Under the crest, a water recirculation region (black area in the figure) exists (cf. Okuda [65]).

As R_B increases, a streaky structure appears, then the windsea surface becomes rough, as demonstrated by Ebuchi *et al.* [62]. In analogy to Shapiro [66],

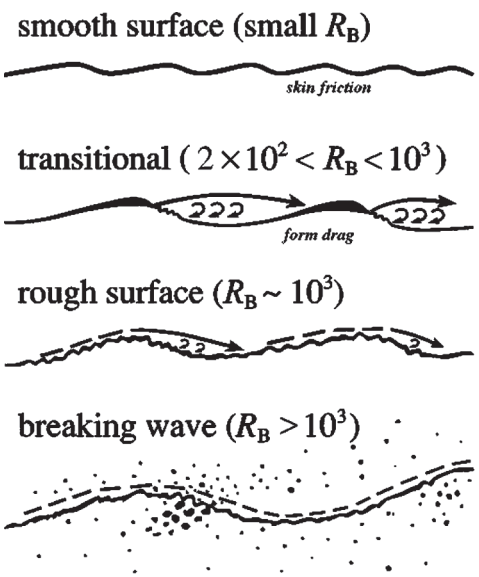

Figure 5: Schematic representation of the regime shift of the windsea boundary layer conditions as a function of R_B.

we hypothesize that the separation point would shift to the windward face of the crest, and the turbulent boundary layer would become thinner with a smaller separation bubble, as illustrated in the third panel of Fig. 5 (about 10^3 in R_B). At this rough-surface stage, C_D would even decrease as shown in Fig. 3 for R_B approaching 10^3. However, because the windsea is composed of various irregular individual wind waves, a sharp decrease in C_D, as shown in the analogous case for a system of golf balls, does not occur and the curve in Fig. 3 is flatter with a slight kink at 10^3 in R_B.

When R_B exceeds 10^3, wave breaking commences as shown by Toba and Koga [5] and Zhao and Toba [6], turbulence breaks the interface, and wind stress, as well as gas transfer, increases drastically, corresponding to the conditions on the right side of Fig. 3. The bottom panel of Fig. 5 illustrates the conditions, $R_B \sim 5 \times 10^3$ or so, corresponding to photographs shown by Koga [64, 67].

As discussed in Section 3, windsea is a special fluid dynamical phenomenon at the air–water interface, where the coupling process between the two boundary layers of air and water is important, and includes elements of the local wind drift, turbulence in the air and water boundary layers, together with the surface wave motion (Toba [3, 4]; Csanady [2]). The wind stress (surface drag) is related to all these processes, including flow separation, pressure distribution, and viscous stress. Consequently, it is very reasonable that the momentum transfer is controlled by the windsea Reynolds number R_B.

Figure 6 shows laboratory observations of tangential stress and total stress (including form drag) by Banner and Peirson [57]. The values of R_B shown in the abscissa were calculated by using their observational data including windsea, and

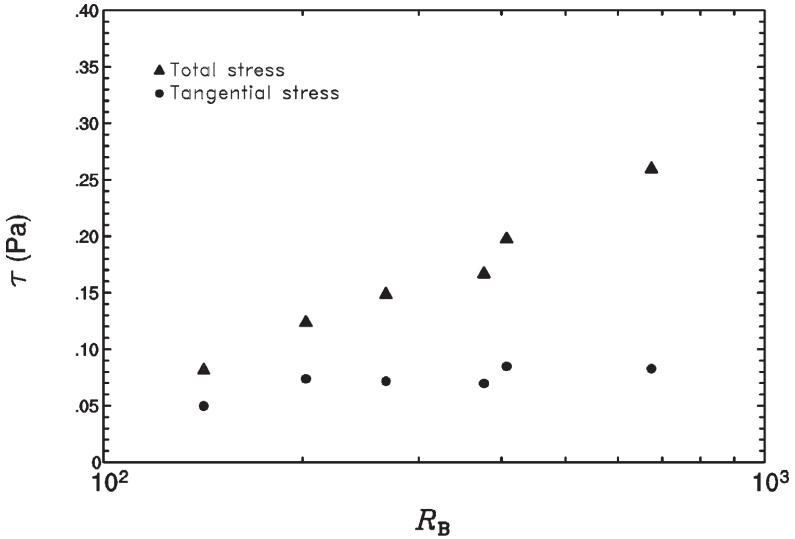

Figure 6: Laboratory observational data of tangential stress and total stress (including form drag) from Banner and Peirson [57]. The values of R_B shown on the abscissa were calculated using their reported data including windsea.

it fortunately ranges between 10^2 and 10^3 in R_B. It is seen that tangential stress stops increasing at 2×10^2, whereas total stress continues to increase. This corresponds to our inference that the shift from the skin friction regime to the form drag regime should occur between the above two critical points.

4.2 Field data: shift of critical point with dynamical contamination

Figure 7 repeats Fig. 3, adding the same data as in Fig. 1, in particular the cluster of points located at the smaller values of u_*/C_p for field observations. The above-mentioned critical point of 10^3 in R_B, seen in Fig. 3, seems to shift to larger values in R_B in the field data in Fig. 7, with C_D tending to be much smaller. C_D thus seems to be an *unstable* quantity that easily changes its character, in the presence of dynamic contamination, such as swells and unsteady winds (see, also Toba *et al.* [38]; chapter 9 of Jones and Toba [10]). Aside from observational errors, this should be the main reason why field observations show so much scatter, and frequently give relatively small values. Figure 8a and b shows the same C_D data expressed against U_{10} or u_*. Note that the data points exhibit much less systematic scatter than appears in Fig. 7.

Figure 7 reminds us of a schematic figure by Shapiro used to explain why golf balls have rough surfaces. Figure 9 is cited from fig. 92 of Shapiro [66]. Shapiro suggested that when the surface of a sphere located in an airflow is smooth, drag first increases with increasing flow speed while the boundary layer is laminar, and there is no flow separation. Flow separation then occurs just behind the shoulder at the

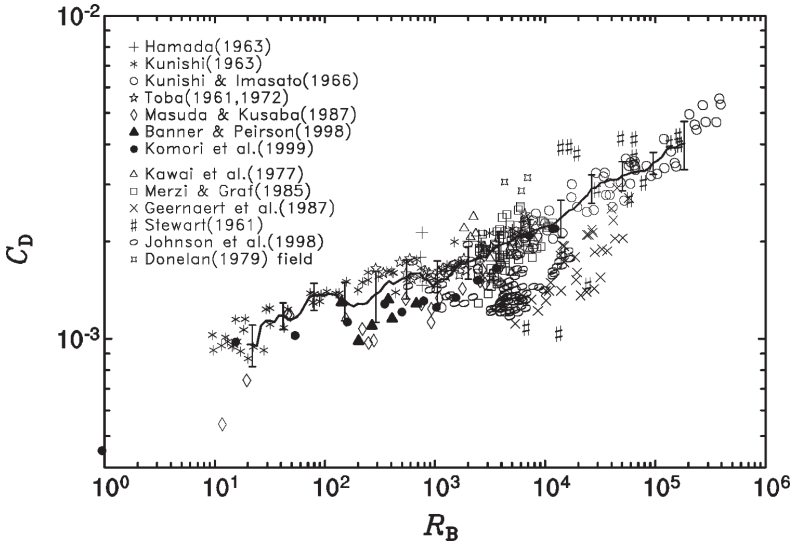

Figure 7: The same data as in Fig. 3, with the addition of the drag coefficient data in Fig. 1 for the cluster of points located at the smaller values of u_*/C_p, corresponding to field observations.

corresponding flow speed. The regime then shifts from laminar to turbulent conditions, and the drag decreases and jumps to another curve for the turbulent boundary layer. At this transition, a thick turbulent boundary layer appears downstream of the separation point. As the flow speed further increases, drag then increases again due to the generation of a wake (see the thin line in Fig. 9).

When the surface of a sphere is rough, the drag is initially larger than that for a smooth surface, because of the form drag due to the roughness. However, the occurrence of flow separation shifts to a lower flow speed, with the separation point shifting upstream of the shoulder, for a thinner turbulent boundary layer. This situation is just the same as illustrated by the third panel in Fig. 5. Though the drag increases again with increasing flow speed, there is a flow speed region (from A to B in Fig. 9) where the drag is smaller for the rough surface case. This region represents the typical speeds at which golf balls travel. The above explanation of Fig. 9 was given as a function of the flow speed in the frame of reference of the moving sphere. However, since golf balls have the same diameter, Fig. 9 can be similarly redrawn with the Reynolds number as the abscissa. This explanation can be extended to the case of the actual sea surface, as discussed above.

For conditions under steady wind without a notable swell component, growing windsea is in local equilibrium with the wind, and the 3/2-power law holds as described in Section 3 (the *wind–windsea equilibrium*). Under unsteady conditions of changing wind speed and direction, the windsea is continuously in the process of adjustment toward the local equilibrium with the ever-changing new wind. For example, an increasing wind causes undersaturation of the high-frequency side

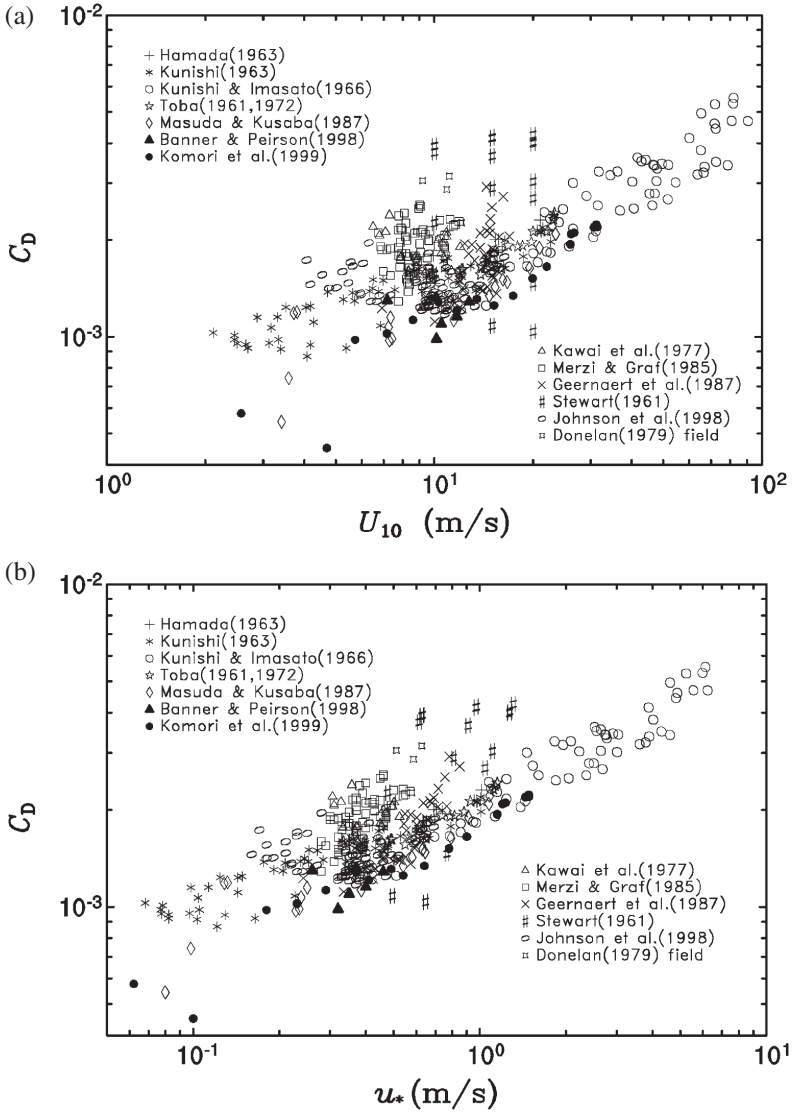

Figure 8: The same data as in Fig. 7 for the drag coefficient, but plotted against (a) U_{10} and (b) u_*.

energy level of the windsea spectrum. Decreasing wind causes oversaturation (Toba *et al*. [37]; Hanson and Phillips [58]). These self-adjustment processes should manifest themselves as amplified fluctuations in C_D. The fluctuations of u_* and C_D thus correspond to under- and oversaturation phenomena (Toba *et al.* [38]).

The existence of conspicuous swell components causes inefficiency in the self-adjustment of windsea to the wind, resulting in smaller values of C_D, as

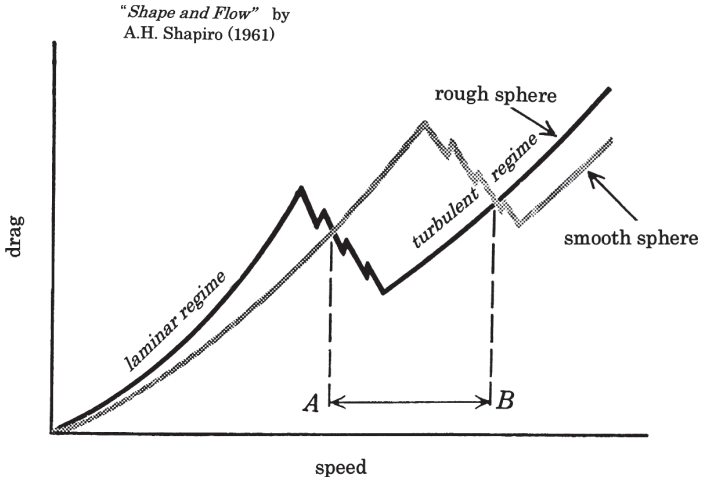

Figure 9: Schematic figure explaining why golf balls have rough surfaces, cited from fig. 92 of Shapiro [66].

demonstrated in Fig. 7. In fact, the existence of swells can cause the wind-wave energy to decrease compared with the pure windsea cases, in a manner reported by Hatori *et al.* [68] and Toba *et al.* [69] (see fig. 22 of Toba [4]). The sea surface would therefore be smoother, in a sense, in the presence of swells, as also reported by Taylor and Yelland [70]. Moreover, Suzuki *et al.* [11] presented the observational data showing reduction in the roughness length z_0 for the same wind, under the existence of swell components in a direction different from the local wind.

C_D itself is thus considered an *unstable quantity*, and nonequilibrium conditions caused by unsteady winds or the existence of significant swells easily act as *dynamic contamination* for the *wind–windsea equilibrium*, resulting in large data scatter in measured C_D values.

5 Nondimensional CO_2 transfer velocity as a function of the windsea Reynolds number

5.1 Nondimensional CO_2 transfer velocity

Both momentum and gas transfers across the sea surface proceed under the existence of wind and windsea. In the windsea boundary layer the laminar–turbulent transition is important, as discussed in Section 4.1. Momentum transfer has been expressed by eqn (2), using the nondimensional drag coefficient C_D, and we have seen that it is primarily controlled by the *windsea Reynolds number*, in situations free of conspicuous swell. Thus, C_D is a measure that can indicate the delicate behavior of momentum transfer caused by the wind and the windsea state.

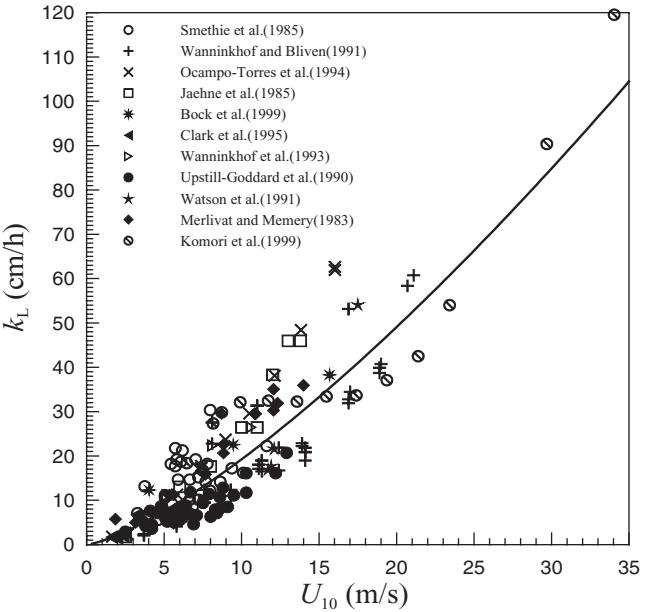

Figure 10: A synthesis of observed values of CO_2 transfer velocity k_L from various sources, cited from Zhao *et al.* [27]. The distribution of data points indicates that k_L already includes the factor for wind proportionality.

On the other hand, gas transfer has so far been treated by using a formulation based on the dimensional gas transfer velocity, k_L. Comparing eqn (5) for the definition of k_L with eqn (2) for that of C_D, we infer that k_L already includes the factor for wind proportionality, as is obviously seen from a synthesis of observed values of k_L in Fig. 10, cited from Zhao *et al.* [27]. This is also inferred theoretically by Fairall *et al.* [13], in relation to their eqn (8).

We therefore propose the nondimensional transfer velocity for CO_2, defined by k_L/U_{10}, namely,

$$F = (k_L/U_{10})U_{10}S\Delta pCO_2. \tag{16}$$

In this way we remove the wind proportionality part, and may extract or amplify the delicate part of the behavior of CO_2 transfer, in order to closely examine the role of the *windsea Reynolds number* R_B, as in the case of C_D.

It should be noted that Zhao *et al.* [27] proposed a formula for k_L as a function of R_B, as one step to the present paper, and Suzuki *et al.* [71] attempted a global mapping of the air–sea CO_2 exchange by using this formula.

5.2 Similarity and dissimilarity between momentum and gas transfers

Figure 11 shows a synthesis of observed values of the nondimensional transfer velocity k_L/U_{10} expressed as a function of R_B, both for laboratory and

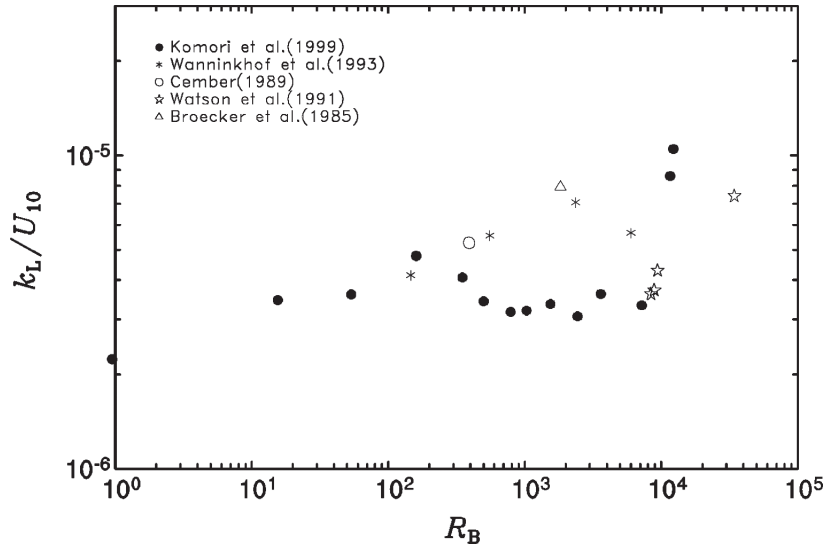

Figure 11: A synthesis of the observed values of the nondimensional transfer velocity k_L/U_{10} expressed as a function of R_B, both for laboratory and field observations.

field observations. The number of data is small; nevertheless we can see important features in the behavior of k_L/U_{10}. As a matter of fact, data sets which included k_L, u_*, the wind speed at a certain level or U_{10} or C_D, and windsea data are very rare. Though more data were included in Fig. 10, some of these, e.g., that of Jähne *et al.* [72], were shown by U_{10} values estimated using an appropriate C_D formula.

In Fig. 11, we first examine the laboratory data obtained by Komori *et al.* [26], shown by closed circles. These data are corrected, using a new calibrating curve, to compensate for errors due to the infrared CO_2 meter that have recently been found by the authors. We see that the k_L/U_{10} values show a decrease between $R_B = 2 \times 10^2$ and 10^3, corresponding to the R_B range where C_D shows a bulge. In the momentum transfer process, the pressure–force mechanism causing the form drag is important, in addition to the tangential stress causing the skin friction, as discussed at the end of Section 4.1 (Fig. 6). In the gas transfer process, however, the mechanism corresponding to the form drag does not exist. As the tangential stress is flat in this range of R_B, the gas transfer velocity should also be flat in the same range. This causes the decrease in k_L/U_{10} as U_{10} increases. This point is the conspicuous difference between the momentum and gas transfer processes.

In Fig. 11, we also see a second critical point beginning at $R_B = 10^3$ and shifting to the right (in R_B) by an order of magnitude, in the field data. This is just as in the case of C_D (Fig. 7).

5.3 Similarity in laboratory and field data relating C_D and k_L

Figure 12 shows k_L/U_{10} plotted as function of C_D. Within the error bars of the data, the laboratory data and the field data seem to coincide with each other. The variation of k_L with C_D is shown in Fig. 13. In this case, the laboratory and the

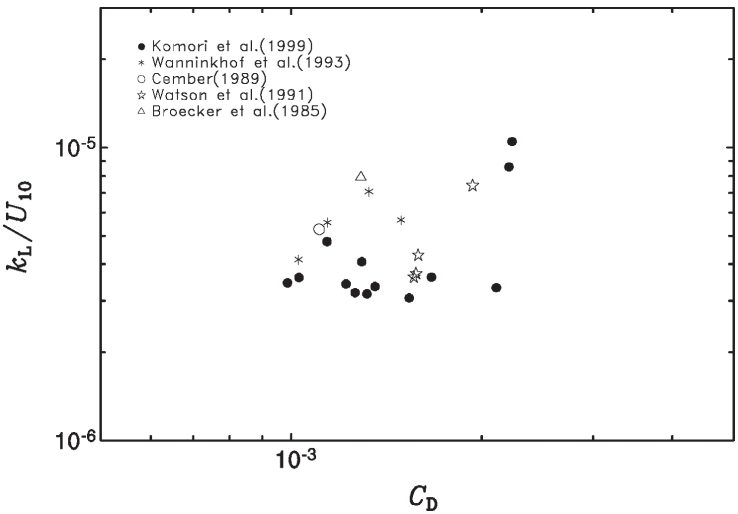

Figure 12: The variation of k_L/U_{10} as a function of C_D. Data sources are same as in Fig. 11.

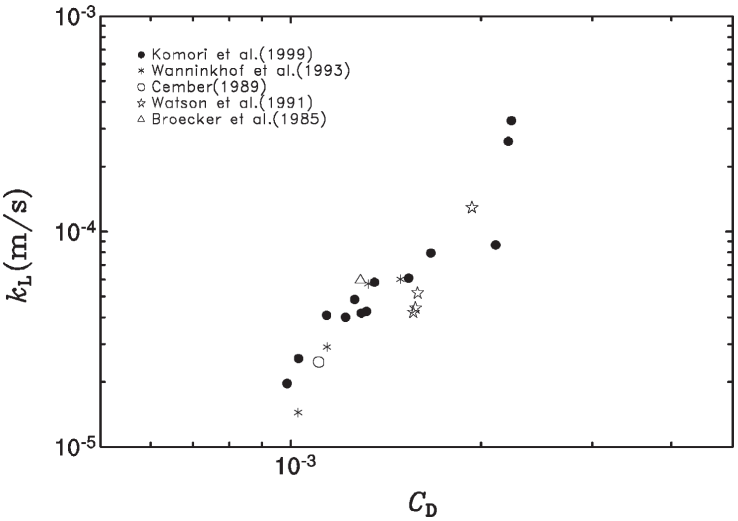

Figure 13: The same data as in Fig. 12, plotting k_L as a function of C_D. Data sources are same as in Fig. 11.

field data show conspicuous agreement with each other. In this figure, the middle relatively flat part of the distribution of data points corresponds to the dissimilarity region in the momentum and gas transfers, between $R_B = 2 \times 10^2$ and 10^3.

We interpret the difference between Figs. 12 and 13 as follows. In all data sets used in these figures, actual U_{10} values were not necessarily measured directly. Rather, we used U_{10} values that had been extrapolated from the wind speed measured at a certain level to 10-m values using the measured stress value with the logarithmic law. This procedure may cause part of the scatter shown in Fig. 11.

In summary, we suggest that there is a fundamental similarity between gas and momentum transfers. This includes our interpretation of the shift of critical points with regard to the *windsea Reynolds number* from laboratory to field data, occurring because of the fluid dynamical smoothing effect due to the intrinsic existence of swell components in the real sea, as discussed for Fig. 9.

6 Conclusions

We have deduced, for the first time, that conditions of windsea-dominant seas can be described by only two nondimensional parameters. One is the *wave age* for the representative windsea, or equivalently the nondimensional significant wave height or wave period, defined by eqn (14), under the existence of the 3/2-power law, eqn (6). The other is the *windsea Reynolds number* R_B, defined by eqn (15). The former describes the degree of windsea development relative to the local wind, whereas the latter is the fundamental controlling parameter for the *windsea boundary layer*, and consequently for the behavior of air–sea transfers.

Though the air–sea CO_2 transfer has traditionally been treated by use of transfer velocity k_L as a function of the 10-m wind speedU_{10}, we propose the use of a nondimensional transfer velocity k_L/U_{10}, in correspondence with the drag coefficient C_D for the momentum transfer. These nondimensional coefficients, k_L/U_{10} and C_D, eliminate the primary wind-speed proportionality part in previous formulations and extract the detailed behavior of the processes of air–sea transfers. There is a fundamental similarity in the behavior of these two nondimensional coefficients, with some dissimilarity in a special range of R_B.

It has been shown that though C_D generally increases with R_B, it has two critical points at $R_B = 2 \times 10^2$ and 10^3 in the pure windsea case, with a flat bulge region between these. The first ($R_B = 2 \times 10^2$) corresponds to the transition from the region where tangential stress prevails, to the occurrence of airflow separation and reattachment to create the form drag. The second ($R_B = 10^3$) is a conspicuous critical point beyond which windsea breaking commences on the fully rough water surface. Namely, it is the transition to the full turbulence regime of the windsea boundary layer. On the other hand, k_L/U_{10} decreases between $R_B = 2 \times 10^2$ and 10^3. This is explained by the fact that in the gas transfer processes, the mechanism corresponding to the pressure–force in the momentum transfer does not exist.

It has also been deduced that field data under usual swell conditions show smaller transfer values or a remarkable shift of the second critical point to larger

values in R_B. This is common for these two nondimensional transfer coefficients, k_L/U_{10} and C_D. This corresponds to the observation that windsea energy becomes small in the presence of swell, especially in a direction different from the wind, which causes the sea surface to be dynamically smoother. In plots of k_L/U_{10} as a function of C_D and k_L as a function of C_D, the distributions of points from windsea tank data and from field data coincide with each other well. These characteristics demonstrate the gross similarity in the momentum and the CO_2 transfers.

Thus, we propose further studies of the behavior of the nondimensional air–sea CO_2 transfer coefficient as a function of R_B. These studies should consider various kinds of swell and unsteady winds. Success in this endeavor would help push our understanding of air–sea fluxes into the mainstream of modern oceanography, in terms of the contemporary evolution of oceanic data acquisition systems with powerful numerical simulations and ocean-wave models.

Acknowledgments

We appreciate the kind encouragement of Dr. William Perrie during this work and his valuable comments on the manuscript. The principal part of this chapter was presented as an invited paper, at a session of the Surface Ocean and Lower Atmosphere Study (SOLAS), convened by Professor Mitsuo Uematsu, within the IUGG General Assembly in Sapporo, July 2003. The authors would like to acknowledge the financial supports by a Grant-in-Aid for Scientific Research (S) (No.14102016) from the Japan Society for the Promotion of Science, and by the 21st Century Center of Excellence Program for Research and Education on Complex Functional Mechanical Systems.

References

[1] Soloviev, A. & Schlüssel, P., Comments on "Air-sea gas transfer: Mechanisms and parameterization". *Journal of Physical Oceanography*, **28**, pp. 1643–1645, 1998.

[2] Csanady, G.T., *Air-Sea Interaction: Laws and Mechanisms*, Cambridge University Press: Cambridge, 2001.

[3] Toba, Y., Similarity laws of the wind wave and the coupling process of the air and water turbulent boundary layers. *Fluid Dynamics Research*, **2**, pp. 263–279, 1988.

[4] Toba, Y., Wind-forced strong wave interactions and quasi-local equilibrium between wind and windsea with the friction velocity proportionality (Chapter 1). *Nonlinear Ocean Waves (Advances in Fluid Mechanics, Vol. 17)*, ed. W. Perrie, Computation Mechanics Publications: Southampton, pp. 1–59, 1998.

[5] Toba, Y. & Koga, M., A parameter describing overall conditions of wave breaking, whitecapping, sea-spray production and wind stress. *Oceanic Whitecaps*, eds E.C. Monahan & G. MacNiocaill, D. Reidel Publishing Company: Dordrecht, pp. 37–47, 1986.

[6] Zhao, D. & Toba, Y., Dependence of whitecap coverage on wind and wind-wave properties, *Journal of Oceanography*, **57**, pp. 603–616, 2001.
[7] Iida, N., Toba, Y. & Chaen, M., A new expression for the production rate of sea water droplets on the sea surface, *Journal of Oceanography*, **48**, pp. 439–460, 1992.
[8] Yelland, M.J., Moat, B.I., Taylor, P.K., Pascal, R.W., Hatchings, J. & Cornell, V.C., Measurements of the open ocean drag coefficient for air flow disturbance by the ship. *Journal of Physical Oceanography*, **28**, pp. 1511–1526, 1998.
[9] Yelland, M.J. & Taylor, P.K., Wind stress measurements from the open ocean. *Journal of Physical Oceanography*, **26**, pp. 541–558, 1996.
[10] Jones, I.S.F. & Toba, Y. (eds). *Wind Stress over the Ocean*, Cambridge University Press: Cambridge, 2001.
[11] Suzuki, N., Ebuchi, N., Zhao, C., Watabe, I. & Sugimori, Y., Study of the relationship between non-dimensional roughness length and wave age, effect by wave directionality. *Proc. Indian Academy of Sciences (Earth and Planetary Sciences)*, **111(3)**, pp. 305–313, 2002.
[12] McGills, W.R., Edson, J.B., Hare, J.E. & Fairall, C.W., Direct covariance air-sea CO_2 fluxes. *Journal of Geophysical Research*, **106**, pp. 16729–16745, 2001.
[13] Fairall, C.W., Hare, J.B., Edson, J.B. & McGillis, W., Parameterization and micrometeorological measurement of air-sea gas transfer. *Boundary-Layer Meteorology*, **96**, pp. 63–105, 2000.
[14] Haubecker, H. & Jähne, B., In situ measurements of the air-sea gas transfer rate during the MBL/CoOP west coast experiment. *Air-Water Gas Transfer*, eds B. Jähne & E. Monahan, AEON: Hanau, pp. 553–569, 1995.
[15] Wanninkhof, R., Asher, W., Weppernig, R., Chen, H., Schlosser, P., Langdon, C. & Sambrotto, R., Gas transfer experiment on Georges Bank using two volatile deliberate tracers. *Journal of Geophysical Research*, **98**, pp. 20237–20248, 1993.
[16] Watson, A.J., Upstill-Goddard, R.C. & Liss, P.S., Air-sea gas exchange in rough and stormy seas measured by a dual-tracer technique. *Nature*, **349**, pp. 145–147, 1991.
[17] Cember, R., Bomb radiocarbon in the Red Sea. *Journal of Geophysical Research*, **94**, pp. 2111–2123, 1989.
[18] Broecker, W.S., Peng, T.H., Ostlund, G. & Stuiver, M. The distribution of bomb radiocarbon in the ocean. *Journal of Geophysical Research*, **90**, pp. 6953–6970, 1985.
[19] Komori, S. & Shimada, T., Gas transfer across a wind-driven air-water interface and the effects of sea water on CO_2 transfer. *Air-Water Gas Transfer*, eds B. Jähne & E. Monahan, AEON: Hanau, pp. 553–569, 1995.
[20] Komori, S. & Misumi, R., The effects of bubbles on mass transfer across the breaking air-water interface. *Gas Transfer at Water Surface*, eds E.S. Saltzman, M. Donelan, W. Drennan & R. Wanninkhof, AGU Monograph, pp. 285–290, 2002.

[21] Liss, P.S. & Merlivat, L., Air-sea gas exchange rates: introduction and synthesis. *The Role of Air-Sea Exchange in Geochemical Cycling*, ed. P. Buat-Menard, D. Reidel Hingham, MA, pp. 113–129, 1986.
[22] Wanninkhof, R., Relationship between wind speed and gas exchange over the ocean, *Journal of Geophysical Research*, **97**, pp. 7373–7382, 1992.
[23] Komori, S., Ueda, H., Ogino, F. & Mizushina, T., Turbulence structure and transport mechanism at the free surface in an open channel flow. *International Journal of Heat and Mass Transfer*, **25**, pp. 513–521, 1982.
[24] Komori, S., Murakami, Y. & Ueda, H., The relationship between surface-renewal and bursting motions in an open-channel flow. *Journal of Fluid Mechanics*, **203**, pp. 103–123, 1989.
[25] Komori, S., Nagaosa, R. & Murakami, Y., Turbulence structure and mass transfer across a sheared air-water interface in wind-driven turbulence. *Journal of Fluid Mechanics*, **249**, pp. 161–183, 1993.
[26] Komori, S., Shimada, T. & Misumi, R., Turbulence structure and mass transfer at a wind-driven air-water interface. *Wind-over-Wave Couplings*, eds S.G. Sajjadi, N.H. Thomas & J.C.R. Hunt, Oxford University Press: New York, pp. 273–285, 1999.
[27] Zhao, D., Toba, Y., Suzuki, Y. & Komori, S., Effect of wind waves on air-sea gas exchange: proposal of an overall CO_2 transfer velocity formula as a function of breaking-wave parameter. *Tellus*, **55B**, pp. 478–487, 2003.
[28] Toba, Y. Chapters 1 and 2. *Ocean-Atmosphere Interactions*, ed. Y. Toba, TERRAPUB/Kluwer: Tokyo/Dordrecht, pp. 1–62, 2003.
[29] Ebuchi, N., Toba, Y. & Kawamura, H., Statistical study on the local equilibrium between wind and wind waves by using data from ocean data buoy stations. *Journal of Oceanography*, **48**, pp. 77–92, 1992.
[30] Johnson, H.K., Hojstrup, H.J., Vested, H.J. & Larsen, S.E., On the dependence of sea surface roughness on wind waves. *Journal of Physical Oceanography*, **28**, pp. 1702–1716, 1998.
[31] Toba, Y., Local balance in the air-sea boundary processes—I. On the growth process of wind waves. *Journal of the Oceanographic Society of Japan*, **28**, pp. 109–120, 1972.
[32] Toba, Y., Stochastic form of the growth of wind waves in a single-parameter representation with physical implications. *Journal of Physical Oceanography*, **8**, pp. 494–507, 1978.
[33] Wilson, B.W., Numerical prediction of ocean waves in the North Atlantic for December 1959. *Dtsch. Hydrogr. Z.*, **18**, pp. 114–130, 1965.
[34] Mitsuyasu, H., Nakamura, R. & Komori, T., Observations of the wind and waves in Hakata Bay. *Rep. Res. Inst. Appl. Mech., Kyushu University*, **19**, pp. 37–74, 1971.
[35] Hasselmann, K., Barnett, T.P., Bouws, E., Carlson, H., Cartwright, D.E., Enke, K., Ewing, J.A., Gienapp, H., Hasselmann, D.E., Kruseman, P., Meerburg, A., Mueller, P., Olbers, D.J., Richter, K., Sell, W. & Walden, H., Measurements of wind-wave growth and swell decay during the Joint North

Sea Wave Project (JONSWAP). *Deut. Hydrogr. Z., Suppl. A*, **8(12)**, 95pp., 1973.

[36] Toba, Y., Iida, N., Kawamura, H., Ebuchi, N. & Jones, I.S.F., Wave dependence of sea-surface wind stress. *Journal of Physical Oceanography*, **20**, pp. 706–721, 1990.

[37] Toba, Y., Okada, K. & Jones, I.S.F., The response of wind-wave spectra to changing winds. Part I. Increasing winds. *Journal of Physical Oceanography*, **18**, pp. 1231–1240, 1988.

[38] Toba, Y., Jones, I.S.F., Ebuchi, N. & Kawamura, H., The role of gustiness in determining the aerodynamic roughness of the sea surface. *The Air-Sea Interface*, eds M.A. Donelan, W.H. Hui & W.J. Plant, University of Miami Press: Miami, pp. 407–412, 1996.

[39] Waseda, T., Toba, Y. & Tulin, M.P., Adjustment of wind waves to sudden changes of wind speed. *Journal of Oceanography*, **57**, pp. 519–533, 2001.

[40] Komatsu, K. & Masuda, A., A new scheme of nonlinear energy transfer among wind waves: RIAM Method—algorithm and performance. *Journal of Oceanography*, **52**, pp. 509–537, 1996.

[41] The WAMDI Group, The WAM model—a third generation ocean wave prediction model. *Journal of Physical Oceanography*, **18**, pp. 1775–1810, 1988.

[42] Suzuki, Y., Development and application of a global ocean wave prediction model including nonlinear interactions and dissipation, PhD Thesis, Graduate School of Science, University of Tokyo, 1995.

[43] Bailey, R.J., Jones, I.S.F. & Toba, Y., The steepness and shape of wind waves, *Journal of the Oceanographic Society of Japan*, **47**, pp. 249–264, 1991.

[44] Tokuda, M. & Toba, Y., Statistical characteristics of individual waves in laboratory wind waves. II. Self-consistent similarity regime. *Journal of the Oceanographic Society of Japan*, **38**, pp. 8–14, 1982.

[45] Toba, Y., Local balance in the air-sea boundary processes—III. On the spectrum of wind waves. *Journal of the Oceanographic Society of Japan*, **29**, pp. 209–220, 1973.

[46] Kawai, S., Okada, K. & Toba, Y., Field data support of the three-seconds power law and the $gu_*\sigma^{-4}$-spectral form for growing wind waves. *Journal of the Oceanographic Society of Japan*, **33**, pp. 137–150, 1977.

[47] Phillips, O.M., Spectral and statistical properties of the equilibrium range of wind generated gravity waves. *Journal of Fluid Mechanics*, **156**, pp. 505–531, 1985.

[48] Zakharov, V.E. & Filonenko, N.N., Energy spectrum for stochastic oscillation of the surface of a liquid. *Doklady Akademii Nauk SSSR*, **170**, pp. 1291–1295, 1966.

[49] Joseph, P.S., Kawai, S. & Toba, Y., Ocean wave prediction by a hybrid model—combination of single-parameterized wind waves with spectrally treated swells. *Tohoku Geophys. J. (Sci. Rep. Tohoku Univ. Ser. 5)*, **28**, pp. 27–45, 1981.

[50] Tulin, M.P., Breaking of ocean waves and downshifting. *Waves and Nonlinear Processes in Hydrodynamics*, eds J. Grue, B. Gjevich & J.E. Weber, Kluwer: Dordrecht, pp. 170–190, 1996.
[51] Mitsuyasu, H. & Honda, T., The high frequency spectrum of wind-generated waves. *Journal of Physical Oceanography*, **30**, pp. 185–198, 1974.
[52] Toba, Y., Suzuki, Y. & Iida, N., Study on global distribution with seasonal variation of the whitecap coverage and sea-salt aerosol production on the sea surface. *The Wind Driven Air-Sea Interface*, ed. M.L. Banner, School of Mathematics, University of NSW, pp. 355–356, 1999.
[53] Monahan, E.C. & MacNiocaill, G. (eds). *Oceanic Whitecaps and Their Role in Air-Sea Exchange Processes*, D. Reidel: Dordrecht, 1986.
[54] Wu, J., Oceanic whitecaps and sea state. *Journal of Physical Oceanography*, **9**, pp. 1064–1068, 1979.
[55] Toba, Y. & Kawamura, H., Wind-wave coupled downward-bursting boundary layer (DBBL) beneath the sea surface. *Journal of Oceanography*, **52**, pp. 409–419, 1996.
[56] Toba, Y. & Kunichi, H., Breaking of wind waves and the sea surface wind stress. *Journal of the Oceanographic Society of Japan*, **26**, pp. 71–80, 1970.
[57] Banner, M. & Peirson, W., Tangential stress beneath wind-driven air-water interfaces. *Journal of Fluid Mechanics*, **364**, pp. 115–145, 1998.
[58] Hanson, J.L. & Phillips, O.M., Wind sea growth and dissipation in the open sea. *Journal of Physical Oceanography*, **29**, pp. 1633–1648, 1999.
[59] Kawai, S., Visualization of airflow separation over wind-wave crests under moderate wind. *Boundary-Layer Meteorology*, **21**, pp. 93–104, 1981.
[60] Kawai, S., Structure of air flow over wind wave crests. *Boundary-Layer Meteorology*, **23**, pp. 503–521, 1982.
[61] Kawamura, H. & Toba, Y., Ordered motion in the turbulent boundary layer over wind waves. *Journal of Fluid Mechanics*, **197**, pp. 105–138, 1988.
[62] Ebuchi, N., Kawamura, H. & Toba, Y., Fine structure of laboratory wind-wave surfaces studied using an optical method. *Boundary-Layer Meteorology*, **39**, pp. 133–151, 1987.
[63] Toba, Y., Drop production by bursting of air bubbles on the sea surface—III. Study by use of a wind flume. *Mem. College of Sci., University of Kyoto*, **A29**, pp. 313–344, 1961.
[64] Koga, M., Direct production of droplets from breaking wind-waves—its observation by a multi-colored overlapping exposure photographing technique. *Tellus*, **33**, pp. 552–563, 1981.
[65] Okuda, K., Internal flow structure of shot wind waves. Part I. On the internal vorticity structure. *Journal of the Oceanographic Society of Japan*, **38**, pp. 28–42, 1982.
[66] Shapiro, A.H., *Shape and Flow*, Educational Services Incorporated, originally published by Doubleday & Co., Inc.: New York, 1961.
[67] Koga, M., Bubble entrainment in breaking wind waves. *Tellus*, **34**, pp. 481–489, 1982.

[68] Hatori, M., Tokuda, M. & Toba, Y., Experimental study on strong interaction between regular waves and wind waves I. *Journal of the Oceanographic Society of Japan*, **37**, pp. 111–119, 1981.
[69] Toba, Y., Hatori, M., Imai, Y. & Tokuda, M., Experimental study of elementary processes in wind-waves using wind over regular waves. *Wave Dynamics and Radio Probing of the Ocean Surface*, eds O.M. Phillips & K. Hasselmann, Plenum: New York, pp. 117–127, 1986.
[70] Taylor, P.K. & Yelland, M.J., The dependence of sea surface roughness on the height and steepness of the waves. *Journal of Physical Oceanography*, **31**, pp. 572–590, 2001.
[71] Suzuki, Y., Komori, S., Zhao, D. & Toba, Y., Global mapping with seasonal variation of air-sea CO_2 exchange by using wind and wind-wave distribution. *Extended Abstracts, 6th International Carbon Dioxide Conference, Sendai*, Vol. II, pp. 756–759.
[72] Jähne, B., Wais, T., Memery, L., Caulliez, G., Merlivat, G.L., Münnich, K.O. & Coantic, M., He and Rn gas exchange experiments in the large wind-wave facility of IMST. *Journal of Geophysical Research*, **90**, pp. 11989–11997, 1985.

Nomenclature

B	Proportionality factor for the 3/2-power law
C_D	Drag coefficient
C_p	Phase speed for peak frequency windsea
C_s	Phase speed for significant waves
f_s	Frequency of appearance of surface-renewal eddies
g	Acceleration due to gravity
H_s	Significant wave height
H^*	Nondimensional significant wave height
k_L	CO_2 transfer velocity
k_s	Significant wave number
S	Solubility of CO_2 in water
T_s	Significant wave period
T^*	Nondimensional significant wave period
$(\overline{u_a'^2})^{1/2}$	Intensity of air turbulence
$(\overline{u_w'^2})^{1/2}$	Intensity of water turbulence
u_0	Stokes drift velocity
u_s	Averaged local wind drift
u_*	Air friction velocity
u_{*w}	Water friction velocity
W	Percentage of whitecap coverage
z_0	Aerodynamic roughness parameter
α	Percentage of breaking crests of individual wind waves
α_s	Coefficient of $gu_*\sigma^{-4}$-type one-dimensional windsea

β	Wave age ($=C_s/u_*$ or C_p/u_*)
ΔpCO_2	Partial pressure difference of CO_2 between air and water
ν	Kinematic viscosity of air
σ	Wave angular frequency
σ_p	Spectral peak angular frequency
τ	Sea-surface wind stress
ϕ	Windsea spectral density
ϕ_p	Windsea spectral density at the peak frequency